Controlling the recombination rate of semiconductor active layers via coupling to dispersion-engineered surface plasmons

John Henson, Anirban Bhattacharyya, Theodore D. Moustakas, and Roberto Paiella*

Department of Electrical and Computer Engineering and Photonics Center, Boston University, 8 St. Mary's Street, Boston, Massachusetts 02215, USA
**Corresponding author: rpaiella@bu.edu*

Received February 22, 2008; revised May 5, 2008; accepted May 6, 2008; posted May 7, 2008 (Doc. ID 93028); published July 28, 2008

The coupling between excited electron-hole pairs in semiconductor active layers and surface plasmon polaritons in metallo-dielectric stacks is investigated. These structures can be used to engineer the surface-plasmon dispersion properties so as to introduce tunable singularities in the photonic density of modes, and hence in the recombination rate of nearby active media. A detailed theoretical study of this effect is presented together with the experimental demonstration of geometrically tunable increased recombination in GaN/AlGaN quantum wells via near-UV photoluminescence measurements. If combined with a suitable geometry to efficiently scatter the emitted surface waves into radiation, this approach can be used for light-emission efficiency enhancement at tunable wavelengths. © 2008 Optical Society of America

OCIS codes: 240.6680, 250.5230.

1. INTRODUCTION

Surface plasmon polaritons (SPPs) at metal/dielectric interfaces are currently the subject of extensive research efforts, motivated by a wide range of applications in the areas of subwavelength integrated optics, sensing, and optoelectronics [1]. This interest stems from the unique optical properties of SPPs, most notably their strongly localized optical fields near the interface and their highly enhanced density of modes near their resonance frequency ω_{SPP}. An important phenomenon directly related to these properties is the ability of metal surfaces to modify the lifetime of nearby light emitters. Specifically, if the surface lies within the near-field of a radiating dipole, the dipole decay rate can be greatly enhanced through the direct excitation of SPPs, particularly if its oscillation frequency closely matches the resonance ω_{SPP}. In the case of an ideally flat metal/dielectric interface, this process leads to a decrease in the intensity of the emitted radiation, since SPPs are guided modes bound to the interface and therefore inherently nonradiative. On the other hand, if the emitted SPPs are efficiently coupled to radiation by a structure providing the required in-plane momentum matching (e.g., a grating), the end result can be a substantial increase in the overall radiative emission rate.

While these phenomena have been known for many years [2–5], they are presently the subject of revived interest due to the emergence of new applications and continuous advances in nanophotonics. Of particular technological importance is the use of SPPs to control the recombination rate of semiconductor active layers [6–12]. This approach was initially demonstrated in [6] through the observation of a pronounced dip in the photoluminescence (PL) of an InGaN/GaN quantum well brought about by a nearby silver film. Subsequently, large PL enhancements mediated by SPPs have been reported with nitride quantum wells [10,11], bulk ZnO [12], and other solid-state systems such as dye-doped polymers [13], silicon quantum dots [14], and erbium-doped glass [15]. SPP-enhanced electroluminescence from a nitride-based light-emitting diode (LED) has also been demonstrated recently [16]. In many of these measurements, efficient coupling of the emitted SPPs to radiation was simply provided by the natural roughness of the metal film, and the size of the observed enhancement (or de-enhancement [6,9,11]) was determined by the interplay between the SPP scattering efficiency and the radiative efficiency of the underlying active layer [17,11]. Other applications of SPP-mediated recombination (not necessarily requiring efficient outcoupling) include increasing the modulation bandwidth of LEDs for short-range optical communications, controlling saturation-induced optical nonlinearities, and laser cooling of solids [18].

A critical requirement for these and other applications of light at metal surfaces is a close match between the SPP resonance and the optical frequency of interest, e.g., the emission frequency in the case of SPP-enhanced recombination. If a single planar metal/dielectric interface is used, ω_{SPP} is entirely determined by the dielectric functions of the two materials across the interface, whose choice is often constrained by other application-specific considerations. Thus, the practical development and broad applicability of many SPP-based technologies will require an effective technique to geometrically tune by design the SPP resonance. Two- and three-dimensional nanostructures, including photonic crystals [7,8], nanoislands [14,15,19], nanospheres [20], and nanoshells [21] are all suitable to this purpose at the expense, however, of

 © 2008 Optical Society of America

increased fabrication complexity. An alternative approach is the use of SPPs in planar metallo-dielectric heterostructures, which allow tailoring the SPP dispersion curves so as to introduce tunable singularities in their density of modes [22,23]. Incidentally, the resulting dispersion-engineered tunable SPPs are also promising for other applications of metal optics ranging from wavelength-specific surface-enhanced sensing to subwavelength waveguiding, slow light, and negative refraction [24,25].

The ability of metallo-dielectric stacks to increase the recombination rate of nearby active layers at tunable wavelengths has first been theoretically investigated in [22]. In that work, the SPP dispersion characteristics were computed by treating all metal films as ideal free-electron gases, and the excitation of these modes by a nearby emissive layer was studied with Fermi's golden rule. This treatment provides a simple and intuitive description of the resulting recombination rate enhancement; however, it does not account for the SPP damping losses in the metals, a simplification which can be expected to limit its quantitative predictive accuracy. To improve upon this initial analysis, here we use a more rigorous theoretical model of fluorescence near metal surfaces [4,5] and we describe all metals by means of their experimentally determined complex dielectric functions [26,27] rather than the elementary Drude response. Furthermore, we present the results of PL measurements with GaN/AlGaN quantum wells coated with suitable metallo-dielectric stacks, showing markedly enhanced recombination (leading to a decrease in the collected light intensity) at tunable wavelengths consistent with simulations. Both theoretical and experimental results confirm the effectiveness of this approach to engineer the SPP dispersion properties and validate its promise for the aforementioned applications, especially if combined with an effective SPP scattering mechanism (e.g., roughness or a grating in the uppermost dielectric layer).

2. THEORY

To illustrate the tunability offered by metallo-dielectric heterostructures, in Fig. 1 we plot the SPP dispersion curves of a single semi-infinite Ag film [Fig. 1(a)] and of a (6 nm)Ag/(9 nm)TiO_2/(25 nm)Au/TiO_2 stack [Fig. 1(b)] deposited on GaN substrates. These curves were computed from Maxwell's equations using the experimental dielectric functions reported in [26] for Ag and Au and in [28] for GaN; for simplicity the imaginary parts of all dielectric functions have been neglected in these calculations (their effect is, however, fully included in the computation of the enhancement factor presented below). As shown in Fig. 1(a), in the case of a single metal film the slope $d\omega/dk$ rapidly increases as the photon energy is decreased below $\hbar\omega_{SPP}$ ($\sim$2.85 eV for Ag on GaN). As a result the SPP density of modes (which is inversely proportional to $d\omega/dk$) and associated emission rate are peaked near $\hbar\omega_{SPP}$, and rapidly drop off away from this resonance. Thus, the use of a single Ag film to increase the recombination rate is suitable for nitride active layers emitting near 2.8–2.9 eV (in the blue-violet spectral region), consistent with experiments [6,9–11,16].

In the case of metallo-dielectric heterostructures such as the Ag/TiO_2/Au/TiO_2 stack of Fig. 1(b), the SPP dispersion curves can be substantially modified by properly selecting the layer thicknesses. In particular, through the mixing and anticrossing of SPP modes localized at neighboring interfaces it is possible to cause a flattening of these curves, and hence singularities in the SPP density of modes, at photon energies that are tunable by design [22]. An example of such flattening is indicated by the circle in Fig. 1(b). The SPP modes within this region are delocalized across the entire stack and have relatively large penetration depths in the GaN light-emitting substrate. (The transverse electric-field component of one of these modes is plotted in the inset.) Combined with the large density of such modes, this leads to a strongly enhanced SPP emission rate in their spectral vicinity (in the green spectral range around 2.4 eV). It should be noted that no single metal film based on materials commonly used with nitride semiconductors could provide a SPP resonance in this spectral region. Furthermore the photon energy of peak enhancement can be tuned over a relatively wide range by varying the thicknesses of the metal and dielectric layers in the stack [22].

The recombination rate enhancement produced by these structures can be determined using a classical model of fluorescence near metal surfaces, which allows computing the emission rates over the entire k-$\hbar\omega$ plane, and which has proven quite accurate in describing a wide range of situations [4,5,7,29]. In this model the emissive layer is treated as a plane of electric dipole sources of fre-

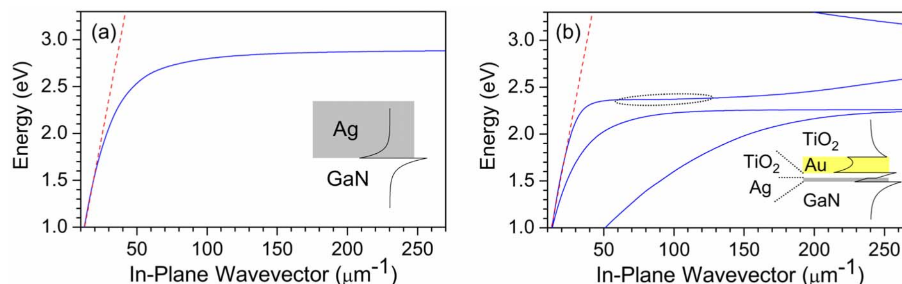

Fig. 1. (Color online) SPP dispersion curves of (a), a single Ag film and (b), a (6 nm)Ag/(9 nm)TiO_2/(25 nm)Au/TiO_2 stack on a GaN substrate. The dashed straight line in each plot is the light line in GaN. Also shown in the inset of each graph is the transverse field component of a representative SPP mode [the mode at $k=80\ \mu m^{-1}$ from the single dispersion curve of (a) and from the curve denoted by the dotted circle in (b)]. These field profiles were computed by solving Maxwell's equations in all layers involved and matching the solutions with the electromagnetic boundary conditions.

quency ω, whose radiated field is Fourier expanded in a sum of plane or evanescent waves over all values of the in-plane wavevector k. For all these component waves, the correspondingly reflected waves from the metallo–dielectric stack are calculated using a matrix technique to account for the multiple interfaces [30], and their amplitudes are then added. The spontaneous emission rate (into both radiative and SPP modes) Γ is then computed as the work-per-unit time done by the dipole on the radiation field, i.e. [4,5],

$$\Gamma = -\frac{\omega}{2}\,\mathrm{Im}(\mathbf{p}^{*}\cdot\mathbf{E}), \tag{1}$$

where $\mathbf{p}$ is the dipole moment and $\mathbf{E}$ the total (emitted plus reflected) field at the dipole location. This rate is finally divided by the same quantity in the absence of any metallo-dielectric layers (Γ_0) to yield the spontaneous-emission-rate enhancement $F \equiv \Gamma/\Gamma_0$ (analogous to the Purcell factor).

The result of this analysis depends on whether the dipoles are perpendicular ($\perp$) or parallel ($\parallel$) to the interfaces and can be written as follows [4,5]:

$$F_{\perp} = \mathrm{Re}\int_0^{\infty} \mathrm{d}k\,\frac{3}{2}\,\frac{(k/k_{\mathrm{sub}})^3}{\sqrt{k_{\mathrm{sub}}^2 - k^2}}(1 + r_p), \tag{2}$$

$$F_{\parallel} = \mathrm{Re}\int_0^{\infty} \mathrm{d}k\,\frac{3}{4}\,\frac{k/k_{\mathrm{sub}}}{\sqrt{k_{\mathrm{sub}}^2 - k^2}}\{(1 + r_s) + [1 - (k/k_{\mathrm{sub}})^2](1 - r_p)\}. \tag{3}$$

Here $k_{\mathrm{sub}} = \omega\sqrt{\varepsilon_{\mathrm{sub}}}/c$ is the wavenumber in the light-emitting substrate, and r_p and r_s are the reflection coefficients describing propagation from the active layer into the metallo-dielectric stack and back into the active layer for p- and s-polarized light. These reflection coefficients are computed numerically using a matrix formalism based on standard Fresnel theory [30] with the experimental dielectric functions of all layers involved [26–28] (including their imaginary parts). Specifically,

$$r_{s(p)} = \frac{\overleftrightarrow{M}_{21}^{s(p)}}{\overleftrightarrow{M}_{11}^{s(p)}}, \tag{4}$$

where $\overleftrightarrow{M}^{s(p)}$ is a 2×2 matrix describing how the complex amplitudes of $s(p)$-polarized forward- and backward-traveling plane waves evolve from the emissive layer to the plane immediately past the last interface in the stack. The detailed procedure and all relevant formulas used to calculate $\overleftrightarrow{M}^{s(p)}$ as a function of k and ω can be found in Section 4.9 of [30]. It should be noted that the resulting reflection coefficients r_p and r_s depend in an exponential fashion on the spacer-layer thickness between the radiating dipoles and the first metallic interface, as they also include the phase and amplitude change due to the round trip in this layer. Finally, if the spontaneous emission rate can be assumed to be isotropic, the overall enhancement factor is given by the average $F = (2F_{\parallel} + F_{\perp})/3$.

Shown in Figs. 2(a) and 2(b) are the results of this analysis for the single Ag film of Fig. 1(a) and for the $Ag/TiO_2/Au/TiO_2$ stack of Fig. 1(b), respectively, assuming an 8 nm GaN spacer between the active layer (e.g., an InGaN quantum well) and the Ag film. Specifically, the log10-scale color maps displayed in these figures give the contribution to $F(\hbar\omega)$ from the component wave of in-plane wavevector k [from the integrands of Eqs. (2) and (3)], plotted as a function of k and $\hbar\omega$. The SPP modes of the dispersion curves of Figs. 1(a) and 1(b) are clearly

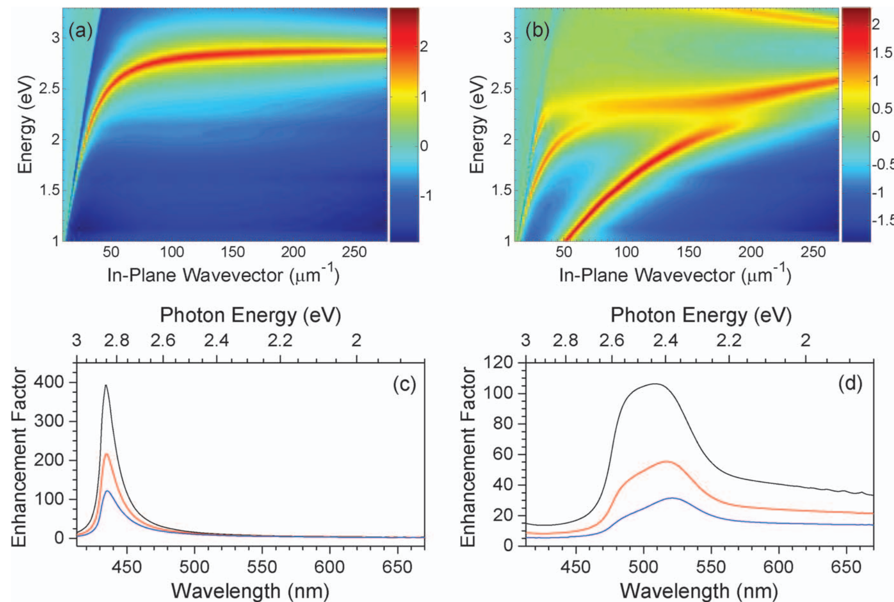

Fig. 2. (a) Spontaneous-emission-rate enhancement factor for a single Ag film on a nitride light-emitting structure, plotted as a log10-scale color map on the k-$\hbar\omega$ plane. (b) Same as (a) for the metallo-dielectric stack of Fig. 1(b). (c) Spontaneous-emission-rate enhancement factor of the single-Ag configuration of (a) integrated over k and plotted versus free-space wavelength λ, assuming a spacer thickness between the active layer and the Ag film of 10, 8, and 6 nm (in order of increasing peak enhancement). (d) Same as (c) for the metallo-dielectric stack of Fig. 1(b). The small periodic modulation observed in the long-wavelength range of (c) and (d) is numerical noise due to the finite grid size used in the integration of (a) and (b).

seen in these figures to produce a large enhancement in the spontaneous emission rate, by an amount that depends on their damping rate and their penetration depth into the emissive layer. The resulting enhancement factors F (integrated over all values of k and plotted versus photon energy $\hbar\omega$ and wavelength λ) are shown in Figs. 2(c) and 2(d) for the structures of Figs. 1(a) and 1(b), respectively, for three different values of the spacer thickness (10, 8, and 6 nm). These curves display a pronounced peak near 2.85 and 2.4 eV (435 and 515 nm), respectively, consistent with the small slope $d\omega/dk$ and hence large SPP density of modes observed in the dispersion curves of Figs. 1(a) and 1(b) at these photon energies. These results therefore clearly illustrate the ability provided by metallo-dielectric heterostructures to control the SPP resonance frequency. At the target photon energy of 2.4 eV of this example, use of the Ag/TiO_2/Au/TiO_2 stack produces a large (up to tenfold) increase in the enhancement factor F compared to the single Ag film case.

In Fig. 3 we show similar results for a (4 nm)Al/(10 nm)HfO_2/(10 nm)Ag/HfO_2 stack on AlGaN, designed for maximum enhancement around 3.5 eV (350 nm) in the near UV. In order to access this relatively high photon-energy range, Al is used as the bottom metal film given its large plasma frequency ($\hbar\omega_{SPP}>5$ eV for Al on AlGaN). Furthermore, HfO_2 is used here instead of TiO_2 because of its larger bandgap, preventing absorption of near-UV light; at the same time both HfO_2 and TiO_2 feature a relatively high dielectric constant, close to that of nitride semiconductors, which is favorable for strong SPP coupling with the nitride substrates. The k-resolved and integrated enhancement factors provided by this stack are plotted in Figs. 3(b) and 3(d), together with those of a single semi-infinite Al film [Figs. 3(a) and 3(c)]. Once again the multiple-layer geometry allows tuning the enhancement peak away from the natural resonance of the single-layer arrangement (~5.2 eV or 240 nm in this case). The peak enhancements shown in this figure are again large enough to produce a substantial change in the recombination rate, although they are smaller than in the previous example due to the larger SPP damping rate in Al compared to Ag. It should also be noted how the anticrossing between the Al and Ag SPP dispersion curves produces a well-defined gap in the local SPP density of modes, and correspondingly a dip in the enhancement factor, which is clearly visible in Fig. 3(d) around 3.3 eV (375 nm).

A further point regarding these simulations that needs to be discussed concerns the upper integration limit k_{upp} used in calculating the traces of Figs. 2(c), 2(d), 3(c), and 3(d). This parameter should not exceed a maximum value that is fundamentally determined by the spatial localization properties of the radiating electron-hole pairs. A measure of such localization is provided by the exciton Bohr radius, which is computed to be about 29 Å in bulk GaN (and smaller in nitride quantum wells) using the standard Coulomb model of excitons [31]: The corresponding maximum k_{upp} value is thus greater than $(29\ \text{Å})^{-1}=340\ \mu\text{m}^{-1}$. In the calculations of Fig. 2 and Fig. 3 we have used the upper integration limits $k_{upp}=275\ \mu\text{m}^{-1}$ and $300\ \mu\text{m}^{-1}$, respectively. These were chosen as large enough so that their exact value does not affect the calculation results in the spectral region of interest in these examples (around 2.4 eV and 3.5 eV, respectively, where the stacks enhancement factors are peaked). At the same time, these values of k_{upp} are well below the fundamental limit just discussed so that their use is fully justified.

Finally, we discuss the relationship between the enhancement factor F introduced in this section and the corresponding change in the overall light emission efficiency,

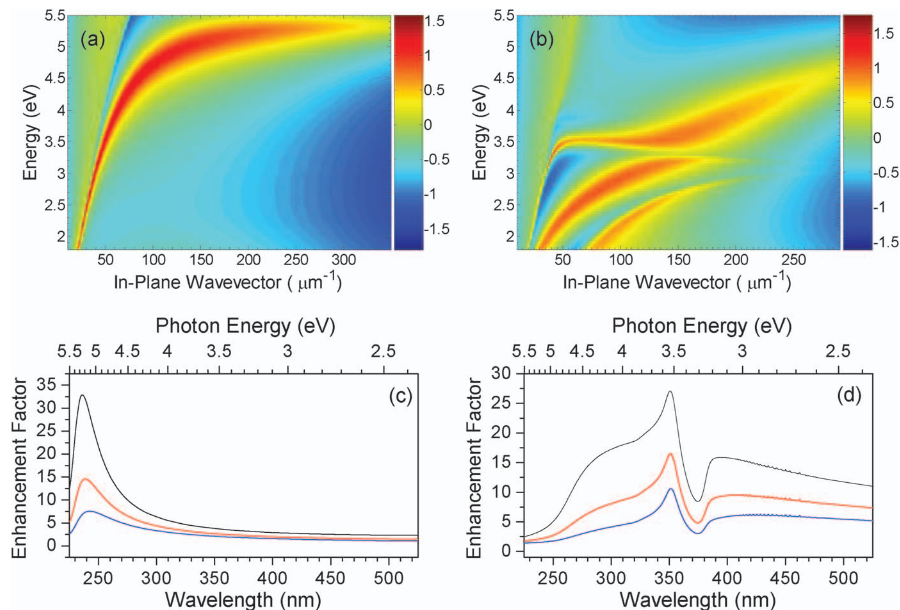

Fig. 3. (a) Spontaneous-emission-rate enhancement factor for a single Al film on a nitride light-emitting structure, assuming a spacer thickness of 8 nm, plotted as a log10-scale color map on the k-$\hbar\omega$ plane. (b) Same as (a) for a (4 nm)Al/(10 nm)HfO_2/(10 nm)Ag/HfO_2 stack. (c) Spontaneous-emission-rate enhancement factor of the single-Al configuration of (a) integrated over k and plotted versus free-space wavelength λ, assuming a spacer thickness between the active layer and the Al film of 10, 8, and 6 nm (in order of increasing peak enhancement). (d) Same as (c) for the metallo-dielectric stack of (b).

which is a more directly accessible and technologically important experimental parameter. In the presence of nearby metal films, light can be radiated both directly and through the excitation and subsequent scattering of SPPs. The resulting (external) efficiency η' can then be written as

$$\eta' = \frac{\Gamma_0'}{\Gamma_0' + \Gamma_{nr} + \Gamma_{SPP}} \eta_{extr}^{rad} + \frac{\Gamma_{SPP}}{\Gamma_0' + \Gamma_{nr} + \Gamma_{SPP}} \eta_{extr}^{SPP}, \quad (5)$$

where Γ_0', Γ_{nr}, and Γ_{SPP} are the recombination rates due to emission of radiation, nonradiative processes, and emission of SPPs, respectively, and η_{extr}^{rad} (η_{extr}^{SPP}) is the extraction efficiency of the emitted photons (SPPs). In the absence of nearby metal films, the light emission efficiency η is

$$\eta = \eta_{int} \eta_{extr}^{rad} = \frac{\Gamma_0}{\Gamma_0 + \Gamma_{nr}} \eta_{extr}^{rad}, \quad (6)$$

where the radiative emission rate Γ_0 is different from that of Eq. (5) (Γ_0') due to the changes in the density of radiation modes brought about by the metallo–dielectric interface. In particular, in the case of an isotropic dipole emitter near a perfect mirror, the ratio Γ_0'/Γ_0 approaches 2/3 if the emitter/mirror separation is small relative to the wavelength [5] (as in all the experimental samples considered in this work).

Using Eqs. (5) and (6) and the definition of the enhancement factor $F = \Gamma/\Gamma_0 = (\Gamma_0' + \Gamma_{SPP})/\Gamma_0$, we find for the SPP-induced change in overall light emission efficiency

$$\frac{\eta'}{\eta} = \frac{\Gamma_0'/\Gamma_0 + (F - \Gamma_0'/\Gamma_0)\, \eta_{extr}^{SPP}/\eta_{extr}^{rad}}{1 + (F-1)\, \eta_{int}}. \quad (7)$$

This expression can be used to identify under what conditions coupling to SPPs leads to an increase versus a decrease in light emission. In particular, in the limit where F is very large the ratio η'/η approaches $\eta_{extr}^{SPP}/(\eta_{int}\eta_{extr}^{rad})$, so that the emission efficiency is enhanced when $\eta_{int}\eta_{extr}^{rad} < \eta_{extr}^{SPP}$. Equation (7) will be used in the next section to relate the measured changes in PL efficiency to the corresponding calculated spontaneous-emission-rate enhancement factors F.

3. EXPERIMENTAL RESULTS

Experimental evidence of the effectiveness of metallo-dielectric stacks to control spontaneous emission has been obtained with GaN/AlGaN quantum-well samples emitting in the near UV. In particular, below we discuss representative data measured with a $GaN/Al_{0.10}Ga_{0.90}N$ single-quantum-well structure on an $Al_{0.30}Ga_{0.70}N$ template layer, grown on c-plane sapphire by molecular beam epitaxy. The GaN well layer has a nominal width of 20 Å and is doped n-type with Si; the upper $Al_{0.10}Ga_{0.90}N$ barrier, which provides the spacer between the radiating dipoles (the quantum confined electron-hole pairs) and the overlaying metals, has a thickness of 10 nm. The metal and dielectric films were deposited over the epitaxial material by electron-beam evaporation, with the deposition rates carefully calibrated in a series of test runs so as to accurately produce the desired thicknesses.

The resulting samples were then characterized via PL measurements with a HeCd pump laser providing about 8 mW of *s*-polarized cw output power at 325 nm. To avoid any complication related to light transmission through the deposited metal and dielectric films, the quantum-well emission was both photoexcited and collected through the sapphire substrate at a grazing angle of about 45°. The emitted light was analyzed with a monochromator with 250-μm-wide slit openings, using an integration time of 250 ms. The contribution to the measured signal due to backscattering of the pump light was found to be minimal in each scan. Temperature-dependent PL measurements were also carried out, with an uncoated sample mounted on the cold finger of a liquid-helium cryostat, in order to evaluate the internal quantum efficiency η_{int} as discussed below.

Shown in Fig. 4(a) are the measured emission spectra of three adjacent pieces from this wafer, one with no metal coverage (dashed-dotted curve), one capped with a single 40-nm-thick Al film (dashed curve), and one coated with a $Al/HfO_2/Ag/HfO_2$ stack aimed at reproducing that of Fig. 3 (solid curve). The control sample with the single Al film (i.e., the bottom film of the stack under study) allows us to identify, from the experimental results, effects related to the SPP dispersion properties of the stack as opposed to effects related to the optical properties of Al and of the Al/AlGaN interface. For example, the contri-

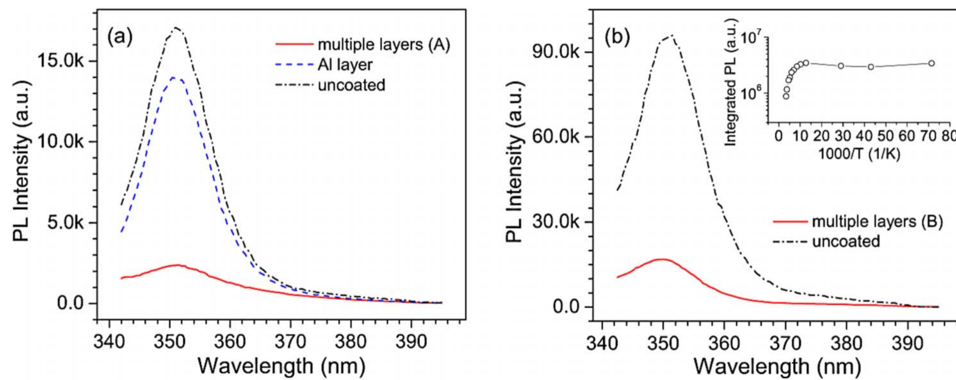

Fig. 4. (Color online) (a) Measured PL spectra of three adjacent samples from the same GaN/AlGaN quantum-well structure: One uncoated, one coated with a single Al film, and one coated with a metallo-dielectric stack designed to reproduce that of Fig. 3. (b) PL spectra of two other adjacent samples from the same wafer: One uncoated and one coated with a similar metallo-dielectric stack (with a thinner Al film). Inset: Arrhenius plot of the integrated PL intensity from a reference uncoated sample.

bution to the measured PL due to SPP scattering can be assumed to be similar in the two coated samples, since the bottom metal/dielectric interface is the same in both samples. It should be noted that, due to the backside pumping geometry used in these measurements, the pumping efficiency is roughly proportional to $1+R$, where R is the power reflection coefficient of the upper surface. This parameter can be taken to be ≈ 1 for the metal-coated samples and ≈ 0.26 for the uncoated reference piece (using Fresnel theory with a refractive index of 2.3 for the nitride substrate [28] and accounting for the 45° angle of incidence from air and s polarization of the pump beam). Thus, for a fairer comparison the emission spectrum of the latter sample in Fig. 4(a) has been multiplied by the factor $(1+1)/(1+0.26)=1.6$.

In Fig. 4(b) the solid curve is the measured PL spectrum of another sample from the same wafer, coated with a similar $Al/HfO_2/Ag/HfO_2$ stack as in Fig. 4(a), except that the deposition time of the Al film was reduced by $\sim 30\%$ (producing an estimated thickness of about 3 nm). For reference, also shown in Fig. 4(b) is a simultaneously measured emission spectrum of an immediately adjacent uncoated piece (dashed-dotted curve), rescaled by a factor of 1.6 as described in the previous paragraph. Qualitatively, the solid line in this figure resembles the corresponding trace of Fig. 4(a). A more detailed comparison, however, reveals evidence of tuning of the spontaneous-emission-rate enhancement spectrum through the geometry of the stack, as discussed below. At the same time, the two reference PL spectra of Figs. 4(a) and 4(b) are essentially identical to each other in shape, which rules out any effect due to possible epitaxial thickness variations on the plane of the wafer.

No SPP-induced light emission efficiency enhancement is observed with these samples, indicating insufficient roughness in the deposited films to effectively scatter the emitted SPPs into radiation. Therefore, the increased recombination rate due to emission of SPPs at the semiconductor/metal interface manifests itself as a decrease in the amount of collected light [6,9,11]. From the data of Fig. 4(a), this effect is significantly stronger in the stack-coated sample compared to the sample with the single Al film, by a factor of about 6 based on the peak values of their respective PL spectra. This indicates that, in the former sample, the excited electron-hole pairs (emitting near 350 nm or 3.5 eV) are more strongly coupled to the nearby SPPs and hence experience a larger recombination-rate enhancement, consistent with the simulation results of Figs. 3(d) and 3(c). To further illustrate this point, in Fig. 5(a) we plot the emission-intensity ratio between the reference uncoated sample and the multiple-layer sample of Fig. 4(a) (solid curve), between the uncoated sample and the multiple-layer sample of Fig. 4(b) (dashed-dotted curve), and between the uncoated sample and the Al-coated sample of Fig. 4(a) (dashed curve). It should be noted that the shapes of these traces closely resemble the theoretical recombination-rate enhancement factors $F(\hbar\omega)$ of Figs. 3(d) (for the multiple-layer samples) and 3(c) (for the Al-coated sample). This is also consistent with expectations [6], since the larger F is, the more SPPs are emitted and (in the present case) eventually lost in the flat metal films, at the expense of radiative waves at the same wavelength.

For a more quantitative comparison between our theoretical and experimental results, we have used the reciprocal of Eq. (7) to calculate the emission-efficiency ratio η/η' between a reference uncoated sample and each coated structure of Fig. 4. These ratios can be expected to accurately reproduce the corresponding emission-intensity ratios of Fig. 5(a), given that the relevant emission-intensity spectra were measured side by side and under the same conditions. The physical parameters required to evaluate Eq. (7) were determined as follows. First, the internal quantum efficiency η_{int} of the uncoated quantum-well material was obtained from the ratio between the measured PL intensities at room temperature and near 10 K [32]. An Arrhenius plot of the integrated PL intensity of a reference uncoated sample is shown in the inset of Fig. 4(b). From these data, an internal quantum efficiency of about 28% is found, which is consistent with previous reports of similar quantum-well structures [33]. Second, the radiative-emission-rate ratio Γ_0'/Γ_0 was taken to be equal to 2/3, as discussed in Section 2 [5]. Third, the extraction-efficiency ratio $\eta_{\mathrm{extr}}^{\mathrm{SPP}}/\eta_{\mathrm{extr}}^{\mathrm{rad}}$ was taken to be zero so as to maximize the calculated emission efficiency de-enhancement η/η' and, correspondingly, optimize the agreement between theoretical and experimental results (see below). This is a reasonable inference, which implies that all metal/dielectric interfaces in our samples lack the degree of roughness required for the efficient scattering of the emitted SPPs into radiation. Finally, the spontaneous-emission-rate enhancement factor F was computed for each coated structure using the formalism described in Section 2. In these calculations the refractive index of the nitride substrate was adjusted to maximize the agreement with the measured data; a value of 2.3 was used, which is reasonable for the alloy composition and carrier density of the experimental samples [28].

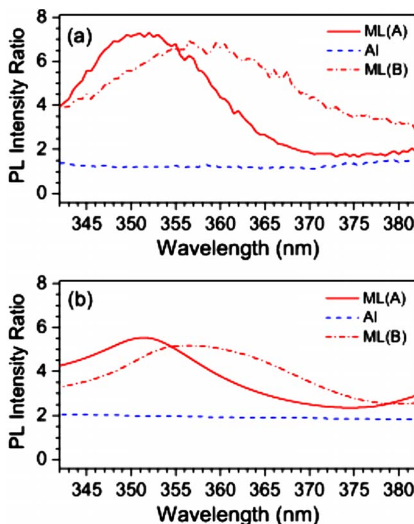

Fig. 5. (Color online) (a) Emission-intensity ratio between the reference uncoated sample and the multiple-layer sample of Fig. 4(a) (solid curve), between the reference sample and the multiple-layer sample of Fig. 4(b) (dashed-dotted curve), and between the reference sample and the Al-coated sample (dashed curve). (b) Theoretical emission-intensity ratios for the three structures of (a), computed as discussed in the text.

The results of this analysis are shown in Fig. 5(b), where the solid curve corresponds to a (4 nm)Al/(10 nm)HfO_2/(10 nm)Ag/HfO_2 stack [as in the multiple-layer sample of Fig. 4(a)]; the dashed-dotted curve corresponds to a (3 nm)Al/(10 nm)HfO_2 /(10 nm)Ag/HfO_2 stack [as in the multiple-layer sample of Fig. 4(b)]; and the dashed line corresponds to a single Al layer. The overall agreement between these theoretical traces and the corresponding experimental curves of Fig. 5(a) is quite remarkable. In particular, the expected resonance peak in the emission-intensity ratio brought about by the Al/HfO_2/Ag/HfO_2 stacks is clearly observed in both theoretical and experimental plots. Furthermore, in both figures this peak undergoes an obvious red shift as the thickness of the Al film is decreased. Quantitatively, the spectral positions of all measured features agree extremely well with the corresponding calculated values. On the other hand, the theoretical peak values are smaller than the experimental ones (which incidentally supports the assumption of negligibly small $\eta_{\mathrm{extr}}^{\mathrm{SPP}}/\eta_{\mathrm{extr}}^{\mathrm{rad}}$ made in our calculations) by $\sim$25%. This discrepancy is, in any case, reasonably small given the many parameters used to evaluate F and η/η', and can be ascribed to uncertainties in these parameters' values. These results therefore fully substantiate the ability of metallo-dielectric heterostructures to tune the resonance of SPPs and, more in general, to engineer their dispersion characteristics.

4. SUMMARY

In conclusion, we have presented a theoretical and experimental study of the coupling between excited electron-hole pairs in semiconductor active layers and SPPs in nanoscale metallo-dielectric stacks. The results indicate that these heterostructures can be effectively used to engineer the SPP dispersion properties so as to introduce tunable singularities in the photonic density of modes. If the optical frequency of such resonances coincides with the emission frequency of nearby radiating dipoles (e.g., electron-hole pairs), their decay (recombination) rate is strongly enhanced. This effect has been investigated with a rigorous theoretical model in which the SPP damping losses in the metals are included explicitly. Experimental evidence of enhanced recombination has then been presented using near-UV light-emitting structures based on III-nitride quantum wells. These results are promising for applications requiring a close match between the optical frequency of interest and the SPP resonance frequency. In particular, if combined with a suitable structure to efficiently scatter the emitted SPPs into radiation (e.g., roughness or a grating in the uppermost dielectric layer), this approach can be used to enhance the light output of low-efficiency light-emitting devices. Additionally, the ability to tailor the SPP dispersion properties described in this work (e.g., to create regions of small or even negative slope) may find novel applications in, e.g., the areas of slow light and negative refraction [24,25,34].

ACKNOWLEDGMENTS

This work was supported by the Department of Energy under grant DE-FG02-06ER46332.

REFERENCES

1. S. A. Maier, *Plasmonics: Fundamentals and Applications* (Springer, 2007).
2. K. H. Drexhage, "Interaction of light with macromolecular dye layers," in *Progress in Optics*, Vol. 12, E. Wolf, ed. (North Holland, 1974), pp. 163–232.
3. R. R. Chance, A. Prock, and R. Silbey, "Molecular fluorescence and energy transfer near interfaces," in *Advances in Chemical Physics*, Vol. XXXVII, I. Prigogine and S. A. Rice, eds. (Wiley, 1978), pp. 1–66.
4. G. W. Ford and W. H. Weber, "Electromagnetic interactions of molecules with metal surfaces," Phys. Rep. **113**, 195–287 (1984).
5. W. L. Barnes, "Fluorescence near interfaces: The role of photonic mode density," J. Mod. Opt. **45**, 661–699 (1998).
6. I. Gontijo, M. Boroditsky, E. Yablonovitch, S. Keller, U. K. Mishra, and S. P. DenBaars, "Coupling of InGaN quantum-well photoluminescence to silver surface plasmons," Phys. Rev. B **60**, 11564–11567 (1999).
7. W. L. Barnes, "Electromagnetic crystals for surface plasmon polaritons and the extraction of light from emissive devices," J. Lightwave Technol. **17**, 2170–2182 (1999).
8. J. Vučković, M. Lončar, and A. Scherer, "Surface plasmon enhanced light-emitting diode," IEEE J. Quantum Electron. **36**, 1131–1144 (2000).
9. A. Neogi, C.-W. Lee, H. O. Everitt, T. Kuroda, A. Tackeuchi, and E. Yablonovitch, "Enhancement of spontaneous recombination rate in a quantum well by resonant surface plasmon coupling," Phys. Rev. B **66**, 153305 (2002).
10. K. Okamoto, I. Niki, A. Shvartser, Y. Narukawa, T. Mukai, and A. Scherer, "Surface-plasmon-enhanced light emitters based on InGaN quantum wells," Nat. Mater. **3**, 601–605 (2004).
11. Y. C. Lu, C. Y. Chen, D. M. Yeh, C. F. Huang, T. Y. Tang, J. J. Huang, and C. C. Yang, "Temperature dependence of the surface plasmon coupling with an InGaN/GaN quantum well," Appl. Phys. Lett. **90**, 193103 (2007).
12. C. W. Lai, J. An, and H. C. Ong, "Surface-plasmon-mediated emission from metal-capped ZnO thin films," Appl. Phys. Lett. **86**, 251105 (2005).
13. T. D. Neal, K. Okamoto, and A. Scherer, "Surface plasmon enhanced emission from dye doped polymer layers," Opt. Express **13**, 5522–5527 (2005).
14. J. S. Biteen, N. S. Lewis, H. A. Atwater, H. Mertens, and A. Polman, "Spectral tuning of plasmon-enhanced silicon quantum dot luminescence," Appl. Phys. Lett. **88**, 131109 (2006).
15. H. Mertens and A. Polman, "Plasmon-enhanced erbium luminescence," Appl. Phys. Lett. **89**, 211107 (2006).
16. D. M. Yeh, C. F. Huang, C. Y. Chen, Y. C. Lu, and C. C. Yang, "Surface plasmon coupling effect in an InGaN/GaN single-quantum-well light-emitting diode," Appl. Phys. Lett. **91**, 171103 (2007).
17. G. Sun, J. B. Khurgin, and R. A. Soref, "Practicable enhancement of spontaneous emission using surface plasmons," Appl. Phys. Lett. **90**, 111107 (2007).
18. J. B. Khurgin, "Surface plasmon-assisted laser cooling of solids," Phys. Rev. Lett. **98**, 177401 (2007).
19. T. R. Jensen, M. D. Malinsky, C. L. Haynes, and R. P. Van Duyne, "Nanosphere lithography: Tunable localized surface plasmon resonance spectra of silver nanoparticles," J. Phys. Chem. B **104**, 10549–10556 (2000).
20. D. D. Evanoff and G. Chumanov, "Synthesis and optical properties of silver nanoparticles and arrays," Chem. Phys. Chem. **6**, 1221–1231 (2005).
21. E. Prodan, C. Radloff, N. J. Halas, and P. Nordlander, "A hybridization model for the plasmon response of complex nanostructures," Science **302**, 419–422 (2003).
22. R. Paiella, "Tunable surface plasmons in coupled metallo-dielectric multiple layers for light-emission efficiency enhancement," Appl. Phys. Lett. **87**, 111104 (2005).
23. J. Chen, N. H. Shen, C. Cheng, Y. X. Fan, J. Ding, and H. T. Wang, "Tunable resonance in surface-plasmon-polariton

enhanced spontaneous emission using a denser dielectric cladding," Appl. Phys. Lett. **89**, 051916 (2006).
24. A. Karalis, E. Lidorikis, M. Ibanescu, J. D. Joannopoulos, and M. Soljacic, "Surface-plasmon-assisted guiding of broadband slow and subwavelength light in air," Phys. Rev. Lett. **95**, 063901 (2005).
25. H. Shin and S. Fan, "All-angle negative refraction for surface plasmon waves using a metal-dielectric-metal structure," Phys. Rev. Lett. **96**, 073907 (2006).
26. P. B. Johnson and R. W. Christy, "Optical constants of noble metals," Phys. Rev. B **6**, 4370–4379 (1972).
27. E. D. Palik, ed., *Handbook of Optical Constants of Solids* (Academic, 1985).
28. D. Brunner, H. Angerer, E. Bustarret, F. Freudenberg, R. Hopler, R. Dimitrov, O. Ambacher, and M. Stutzmann, "Optical constants of epitaxial AlGaN films and their temperature dependence," J. Appl. Phys. **82**, 5090–5096 (1997).
29. J. Bao, N. Yu, F. Capasso, T. Mates, M. Troccoli, and A. Belyanin, "Controlled modification of erbium lifetime in silicon dioxide with metallic overlayers," Appl. Phys. Lett. **91**, 131103 (2007).
30. A. Yariv and P. Yeh, *Photonics: Optical Electronics in Modern Communications* (Oxford U. Press, 2007), Chap. 4.
31. S. L. Chuang, *Physics of Optoelectronic Devices* (Wiley, 1995), Chap. 13.
32. Y. Kawakami, K. Omae, A. Kaneta, K. Okamoto, T. Izumi, S. Saijou, K. Inoue, Y. Narukawa, T. Mukai, and S. Fujita, "Radiative and nonradiative recombination processes in GaN-based semiconductors," Phys. Status Solidi A **183**, 41 (2001).
33. J. S. Cabalu, A. Bhattacharyya, C. Thomidis, I. Friel, T. D. Moustakas, C. J. Collins, and Ph. Komninou, "High power ultraviolet light emitting diodes based on GaN/AlGaN quantum wells produced by molecular beam epitaxy," J. Appl. Phys. **100**, 104506 (2006).
34. H. J. Lezec, J. A. Dionne, and H. A. Atwater, "Negative refraction at visible frequencies," Science **316**, 430 (2007).